PHYSICAL REVIEW B **84**, 085144 (2011)

GW calculations including spin-orbit coupling: Application to Hg chalcogenides

R. Sakuma,[1,2,*] C. Friedrich,[3] T. Miyake,[2,4] S. Blügel,[3] and F. Aryasetiawan[1,2]

[1]*Graduate School of Advanced Integration Science, Chiba University, Chiba 263-8522, Japan*

[2]*Nanosystem Research Institute, National Institute of Advanced Industrial Science and Technology, Tsukuba, Ibaraki 305-8568, Japan*

[3]*Peter Grünberg Institut and Institute for Advanced Simulation, Forschungszentrum Jülich and JARA, D-52425 Jülich, Germany*

[4]*JST, Core Research for Evolutional Science and Technology (CREST), Kawaguchi, Saitama 332-0012, Japan*

(Received 30 June 2011; published 30 August 2011)

We present self-energy calculations for Hg chalcogenides (HgX, X = S, Se, and Te) with inverted band structures using an explicit spin-dependent formulation of the GW approximation. Spin-orbit coupling is fully taken into account in calculating the single-particle Green function G and the screened interaction W. We have found, apart from an upward shift of the occupied conductionlike Γ_6 state by about 0.7 eV, an enhancement of spin-orbit splitting by about 0.1 eV, in good agreement with experiment. This renormalization originates mainly from spin-orbit induced changes in G rather than W, which is affected only little by spin-orbit coupling.

DOI: 10.1103/PhysRevB.84.085144 PACS number(s): 71.15.−m, 71.20.−b, 71.70.Ej

I. INTRODUCTION

Owing to the spin-orbit coupling, the spin of an electron that is propagating through a material with structure or bulk inversion asymmetry interacts with the orbital motion through space in a way as if a momentum-dependent magnetic field was applied. This gives rise to a number of exciting phenomena such as the Dresselhaus[1] and Bychkov-Rashba[2] effect as well as to a number of recent discoveries such as the spin Hall[3] and quantum spin Hall effect[4] as well as two- and three-dimensional topological insulators.[5] These spin-orbit related phenomena opened a new alternative vista for spintronics and unleashed a world-wide effort to search for appropriate materials and to understand their electronic and transport properties. Although only very few topological insulator materials are known, many materials have been suggested to have the potential to be topological insulators.[6–10] The focus is on materials composed of atoms with high atomic numbers such as mercury, thallium, lead, or bismuth, as electrons traveling through these materials are expected to exhibit a strong spin-orbit interaction. One such material class is the mercury chalcogenides, HgX (X = S, Se, and Te). For instance, the key experiment[4] revealing for the first time the two-dimensional quantum spin Hall effect was carried out on a HgTe quantum well after it had been predicted to be a two-dimensional topological insulator.[11]

While the spin-orbit coupling is of atomic origin and is believed to be well described within the one-particle picture with some effective potential, such as the local-density approximation (LDA) of density-functional theory (DFT), the modification of the band structure near the Fermi energy due to the spin-orbit coupling can lead to intriguing phenomena including many-body effects: an interesting example is the recently discovered Ir-based spin-orbit induced Mott insulators,[12–14] in which the spin-orbit splitting as well as electron correlation are essential in determining the electronic properties.

In this work, we investigate the effect of the spin-orbit coupling on quasiparticle calculations within the GW approximation (GWA).[15–17] Because of the coupling of spin and spatial degrees of freedom, spin is not a good quantum number anymore and the Hamiltonian acquires terms that are nondiagonal in spin giving rise to one-particle wave functions that exhibit spatially dependent spin expectation values. This dependence can be expressed by spinor wave functions consisting of nonzero spin-up and spin-down components. Likewise, the Green function and self-energy exhibit additional mixed spin components. Explicit formulas have recently been derived[18,19] for a general spin-dependent electron-electron interaction. The generalization provides, as a special case, a framework to treat systems with inherent spin dependence, such as spin-orbit coupling or spin-spiral structures. A similar approach was recently used to study the effect of spin-orbit coupling on the quasiparticle lifetime.[20,21]

In this work, we apply the spin-dependent GWA to mercury chalcogenides HgX (X = S, Se, and Te) within the full-potential linearized augmented-plane-wave (FLAPW) method, which treats core and valence electrons on the same footing. Mercury chalcogenides, which crystallize in the zinc-blende structure typical for III-V and II-VI compound semiconductors, are prototype materials with a so-called inverted band structure, a property pertinent to realize spin-Hall insulators[22] or strong topological insulators.[23] In these materials the twofold degenerate Γ_6 band, which forms a conduction band in conventional zinc-blende semiconductors, lies below the fourfold degenerate Γ_8 bands and sometimes even below the twofold degenerate split-off Γ_7 bands. Apart from the fundamental theoretical interest related to the quantum spin-Hall effect and topological insulators, these materials are of theoretical interest because the LDA does not reproduce the band structure quantitatively: the inverse band gap in the LDA is overestimated by about 1 eV, and the spin-orbit splitting is about 0.1 eV too small with respect to experiment.

While in previous GW studies of these materials[24,25] the spin-orbit splitting was treated within LDA and added *a posteriori* to the quasiparticle spectrum as a perturbative correction, we use the full four-component spinor wave functions for the GW calculations in this work. In this way, not only the inverse band gaps, but also the spin-orbit splittings are corrected by the self-energy. As a result, apart from a definite quantitative improvement of the direct inverse gaps, we find a hitherto unknown renormalization of the spin-orbit splitting,

which is mainly attributed to spin-orbit induced changes in the single-particle Green function. The resulting spin-orbit splitting compares well with experiment.

II. METHOD

Our approach is based on the fully spin-dependent GWA, Refs. 18 and 19, applied to the case of a spin-independent electron-electron interaction. We consider a many-body Hamiltonian with a spin-dependent one-particle part h^0 and the bare Coulomb interaction $V(r) = 1/r$,

$$H = \sum_i h^0(\mathbf{r}_i, s_i) + \frac{1}{2}\sum_{i\neq j} V(|\mathbf{r}_i - \mathbf{r}_j|). \tag{1}$$

The one-particle part can contain any arbitrary spin-dependent term, indicated by the spin variable s_i, and in this work we include the spin-orbit interaction, which is primarily a one-particle phenomenon. Nonlocal spin-spin and spin-charge (Lorentz) interactions as well as relativistic retardation effects are neglected. Here and in the following, we employ atomic units unless noted otherwise.

Due to the coupling of spin and spatial degrees of freedom, the Green function and the self-energy are no longer diagonal in spin space, but must be written as 2×2 matrices. The Bloch wave function of Bloch vector $\mathbf{k}$ and band index μ is written as

$$\phi_{\mathbf{k}\mu}(\mathbf{r}, s) = \phi^+_{\mathbf{k}\mu}(\mathbf{r})\chi_+(s) + \phi^-_{\mathbf{k}\mu}(\mathbf{r})\chi_-(s), \tag{2}$$

where s is the spin variable, which can take only two values, and $\chi_\pm$ are the spin basis functions, which are chosen to be the eigenfunctions of $\hat{s}_z$, the z component of the spin operator. The Green function of the noninteracting system is given by

$$G(\mathbf{r}s, \mathbf{r}'s'; \omega) = \sum_{\mathbf{k}\mu} \frac{\phi_{\mathbf{k}\mu}(\mathbf{r}, s)\phi^*_{\mathbf{k}\mu}(\mathbf{r}', s')}{\omega - \epsilon_{\mathbf{k}\mu} + i\eta\,\mathrm{sgn}(\epsilon_{\mathbf{k}\mu} - \epsilon_\mathrm{F})}, \tag{3}$$

and the matrix elements in the spin basis are

$$G_{\alpha\beta}(\mathbf{r}, \mathbf{r}'; \omega) = \sum_{\mathbf{k}\mu} \frac{\phi^\alpha_{\mathbf{k}\mu}(\mathbf{r})\phi^{\beta *}_{\mathbf{k}\mu}(\mathbf{r}')}{\omega - \epsilon_{\mathbf{k}\mu} + i\eta\ \mathrm{sgn}(\epsilon_{\mathbf{k}\mu} - \epsilon_\mathrm{F})}, \tag{4}$$

where $\alpha, \beta = \pm$ are the indices of the spin basis functions, η is a positive infinitesimal, ϵ_F is the Fermi energy, and $\epsilon_{\mathbf{k}\mu}$ are the eigenenergies corresponding to the Bloch functions of Eq. (2). We employ the Kohn-Sham system within the LDA as the reference one-particle system. The fully spin-dependent GW self-energy is written as[18,19]

$$\Sigma_{\alpha\beta}(\mathbf{r}, \mathbf{r}'; \omega) = \frac{i}{2\pi}\int G_{\alpha\beta}(\mathbf{r}, \mathbf{r}'; \omega + \omega')W(\mathbf{r}, \mathbf{r}'; \omega')e^{i\eta\omega'}d\omega', \tag{5}$$

where the screened Coulomb interaction W is calculated from the polarization function

$$P(\mathbf{r}, \mathbf{r}'; \omega) = \frac{-i}{2\pi}\sum_{\alpha\beta}\int G_{\alpha\beta}(\mathbf{r}, \mathbf{r}'; \omega + \omega')G_{\beta\alpha}(\mathbf{r}', \mathbf{r}; \omega')d\omega' \tag{6}$$

and the bare Coulomb interaction, which are related by the Dyson-type equation $W = V + VPW$. Although W does not depend on spin explicitly, it is affected by the spin-orbit coupling through the Green function in Eq. (4). The self-energy, Eq. (5), is affected directly through G and indirectly through W. The off-diagonal spin components of the Green function are responsible for the off-diagonal elements of the self-energy.

The quasiparticle wave function $f_{\mathbf{k}\mu}$ satisfies the quasiparticle equation

$$\int d^3r' \sum_\beta \big[\delta(\mathbf{r} - \mathbf{r}')[h^0_{\alpha\beta}(\mathbf{r}) + v^\mathrm{H}(\mathbf{r})\delta_{\alpha\beta}] + \Sigma_{\alpha\beta}(\mathbf{r}, \mathbf{r}', E_{\mathbf{k}\mu})\big]f^\beta_{\mathbf{k}\mu}(\mathbf{r}') = E_{\mathbf{k}\mu}f^\alpha_{\mathbf{k}\mu}(\mathbf{r}), \tag{7}$$

where $v^\mathrm{H}(\mathbf{r})$ is the Hartree potential. In this work, we calculate the quasiparticle energy $E_{\mathbf{k}\mu}$ within the so-called one-shot GW approach, in which one approximates $f^\alpha_{\mathbf{k}\mu} \approx \phi^\alpha_{\mathbf{k}\mu}$ within first-order perturbation theory leading to

$$E_{\mathbf{k}\mu} = \epsilon_{\mathbf{k}\mu} + \sum_{\alpha\beta}\langle\phi^\alpha_{\mathbf{k}\mu}|\Sigma_{\alpha\beta}(E_{\mathbf{k}\mu}) - v^\mathrm{xc}\delta_{\alpha\beta}|\phi^\beta_{\mathbf{k}\mu}\rangle, \tag{8}$$

where $v^\mathrm{xc}(\mathbf{r})$ is the exchange-correlation potential, which is spin-independent for a nonmagnetic system and approximated by the LDA in this work. In previous GW calculations,[24,25] the spin-orbit coupling was not taken into account in the solution of Eq. (8), i.e., neither in the self-energy nor in the Kohn-Sham states and energies. It entered only as an additive perturbative correction to the quasiparticle energies. Spin-off-diagonal terms of the Green function (and all quantities derived from it) describing spin-flip processes due to the spin-orbit interaction were thus ignored.

We have implemented the fully spin-dependent GW approximation according to Eqs. (5), (6), and (8) into the GW code SPEX,[26] which is based on the FLAPW method. In the code, two-particle quantities are expanded in the spin-independent mixed product basis set $\{M_{\mathbf{q}I}(\mathbf{r})\}$. For the exchange part of the self-energy in Eq. (5), we can perform the integration over frequency analytically by summing over the residues, which gives

$$\begin{aligned}
&\langle\phi^\alpha_{\mathbf{k}\mu}|\Sigma^\mathrm{x}_{\alpha\beta}|\phi^\beta_{\mathbf{k}\mu}\rangle \\
&= \frac{i}{2\pi}\sum_{\mathbf{q}\nu}\sum_{I,J}\langle\tilde{M}_{\mathbf{q}J}\phi^\alpha_{\mathbf{k}\mu}|\phi^\alpha_{\mathbf{k}+\mathbf{q}\nu}\rangle\langle\tilde{M}_{\mathbf{q}I}\phi^\beta_{\mathbf{k}\mu}|\phi^\beta_{\mathbf{k}+\mathbf{q}\nu}\rangle^* \\
&\quad\times\int d\omega'\frac{V_{IJ}(\mathbf{q})e^{i\eta\omega'}}{\omega + \omega' - \epsilon_{\mathbf{k}+\mathbf{q}\nu} + i\eta\,\mathrm{sgn}(\epsilon_{\mathbf{k}+\mathbf{q}\nu} - \epsilon_\mathrm{F})} \\
&= -\sum_{\mathbf{q}\nu}\sum_{I,J}\theta(\epsilon_\mathrm{F} - \epsilon_{\mathbf{k}+\mathbf{q}\nu}) \\
&\quad\times\langle\tilde{M}_{\mathbf{q}J}\phi^\alpha_{\mathbf{k}\mu}|\phi^\alpha_{\mathbf{k}+\mathbf{q}\nu}\rangle V_{IJ}(\mathbf{q})\langle\tilde{M}_{\mathbf{q}I}\phi^\beta_{\mathbf{k}\mu}|\phi^\beta_{\mathbf{k}+\mathbf{q}\nu}\rangle^*,
\end{aligned} \tag{9}$$

where $V_{IJ}(\mathbf{q}) = \langle M_{\mathbf{q}I}|V|M_{\mathbf{q}J}\rangle$ is the matrix element of the Coulomb interaction[27] and $\{\tilde{M}_{\mathbf{q}I}\}$ is the biorthogonal set of $\{M_{\mathbf{q}I}\}$. The corresponding expression for the correlation part of the self-energy, obtained by replacing $V_{IJ}(\mathbf{q})$ in the frequency integral of Eq. (9) with $W^\mathrm{c}_{IJ}(\mathbf{q}, \omega') = W_{IJ}(\mathbf{q}, \omega') - V_{IJ}(\mathbf{q})$, requires an explicit integration over frequency, for which we use the contour integration technique.

The polarization function P is calculated as

$$P_{IJ}(\mathbf{q},\omega) = \sum_{\alpha\beta}\sum_{\mathbf{k}\mu\nu}\theta(\epsilon_F-\epsilon_{\mathbf{k}\mu})\theta(\epsilon_{\mathbf{k}+\mathbf{q}\nu}-\epsilon_F) \times\langle\tilde{M}_{\mathbf{q}J}\phi^{\alpha}_{\mathbf{k}\mu}|\phi^{\alpha}_{\mathbf{k}+\mathbf{q}\nu}\rangle\langle\tilde{M}_{\mathbf{q}J}\phi^{\beta}_{\mathbf{k}\mu}|\phi^{\beta}_{\mathbf{k}+\mathbf{q}\nu}\rangle^* \times\left[\frac{1}{\omega-\Delta_{\mathbf{k}\mu\nu}(\mathbf{q})+i\eta}-\frac{1}{\omega+\Delta_{\mathbf{k}\mu\nu}(\mathbf{q})-i\eta}\right], \tag{10}$$

where $\Delta_{\mathbf{k}\mu\nu}(\mathbf{q}) = \epsilon_{\mathbf{k}+\mathbf{q}\nu}-\epsilon_{\mathbf{k}\mu}$ and time-reversal symmetry has been employed.

Using spatial symmetry of the system greatly accelerates the computation and saves memory: the wave functions in the full Brillouin zone are generated from those at the corresponding symmetry-equivalent $\mathbf{k}$ points in the irreducible Brillouin zone, by operating a spatial rotation and also a 2×2 unitary rotation in spin space; symmetry is also exploited in computing P and Σ to reduce the number of $\mathbf{k}$ points appearing in the sum, as described in Ref. 26.

We first prepare well-converged LDA wave functions and energies with the FLAPW DFT code FLEUR,[28] employing the Perdew-Zunger parametrization of the LDA exchange-correlation functional.[29] In the FLEUR code, the core electrons are treated fully relativistically by solving the Dirac equation in the spherically averaged effective potential around each atomic nucleus. For the valence electrons, space is partitioned into nonoverlapping muffin-tin spheres, which are centered at the atomic nuclei, and the interstitial region. Different basis representations are used in the two regions of space (see below). In the interstitial region, relativistic effects are neglected, as they amount to only about 1% of the total relativistic contribution. However, in the muffin-tin spheres, all relativistic effects (e.g., the relativistic mass enhancement to any order in the speed of light) are included, combining the scalar-relativistic approximation[30] with a fast self-consistent nonperturbative treatment of the spin-orbit coupling[31] employing the second-variation technique.[32] In second variation one performs a first diagonalization of the scalar-relativistic (spin-orbit-free) Hamiltonian and, then, diagonalizes the fully relativistic Hamiltonian, including the spin-orbit coupling term v_{SOC}, in the basis of the scalar-relativistic eigenfunctions $\varphi^{\alpha}_{\mathbf{k}n}(\mathbf{r})$, which yields the fully relativistic (i.e., with spin-orbit interaction) solutions

$$\phi_{\mathbf{k}\mu}(\mathbf{r},s) = \sum_{\alpha}\sum_{n} Z^{\alpha}_{n\mu}(\mathbf{k})\varphi^{\alpha}_{\mathbf{k}n}(\mathbf{r})\chi_{\alpha}(s). \tag{11}$$

The band index n comprises at least all states that are later used in the GW calculation. This yields sufficient variational freedom for the spin-orbit coupling term by far. The $\varphi^{\alpha}_{\mathbf{k}n}(\mathbf{r})$ are expanded in terms of the LAPW basis, i.e.,

$$\varphi^{\alpha}_{\mathbf{k}n}(\mathbf{r}) = \frac{1}{\sqrt{\Omega}}\sum_{\mathbf{G}} c^{\alpha}_{\mathbf{k}n,\mathbf{G}}e^{i(\mathbf{k}+\mathbf{G})\cdot\mathbf{r}} \tag{12}$$

with the unit-cell volume Ω in the interstitial region and

$$\varphi^{\alpha}_{\mathbf{k}n}(\mathbf{r}) = \sum_{\mathbf{G}} c^{\alpha}_{\mathbf{k}n,\mathbf{G}}\sum_{lm}\left[a^{\alpha}_{alm}(\mathbf{G},\mathbf{k})u^{\alpha}_{al}(r) + b^{\alpha}_{alm}(\mathbf{G},\mathbf{k})\dot{u}^{\alpha}_{al}(r)\right]Y_{lm}(\hat{\mathbf{r}}) = \sum_{lm}\left[A^{\alpha}_{alm,n}(\mathbf{k})u^{\alpha}_{al}(r) + B^{\alpha}_{alm,n}(\mathbf{k})\dot{u}^{\alpha}_{al}(r)\right]Y_{lm}(\hat{\mathbf{r}}) \tag{13}$$

inside the muffin-tin sphere of atom a, where $\mathbf{r}$ is measured from the sphere center. Here the eigenvectors $c^{\alpha}_{\mathbf{k}n,\mathbf{G}}$ are obtained by diagonalizing the scalar-relativistic Hamiltonian, and the LAPW coefficients $a^{\alpha}_{alm}(\mathbf{G},\mathbf{k})$ and $b^{\alpha}_{alm}(\mathbf{G},\mathbf{k})$ are determined such that the wave functions and their radial derivatives are continuous at the muffin-tin sphere boundaries. The radial functions $u^{\alpha}_{al}(r)$ and $\dot{u}^{\alpha}_{al}(r)$ are the solution of the radial scalar-relativistic Dirac equation[30] and its energy derivative, respectively. They consist of a large (L) and a small (S) component

$$u^{\alpha}_{al}(r) = \begin{pmatrix} u^{\mathrm{L}\alpha}_{al}(r) \\ -i\sigma_r u^{\mathrm{S}\alpha}_{al}(r)\end{pmatrix} \tag{14}$$

with $\sigma_r = \boldsymbol{\sigma}\cdot\boldsymbol{r}/r$, where $\boldsymbol{\sigma}$ is the vector of Pauli spin matrices, and analogously for $\dot{u}^{\alpha}_{al}(r)$. The small component becomes negligible at the muffin-tin sphere boundary.

The basis can be extended by local orbitals to describe semicore states[33] and high-lying unoccupied states,[34,35] which is important to obtain converged GW results.[36] In the basis of the scalar-relativistic eigenfunctions the spin-orbit coupling term is given by

$$\langle\varphi^{\alpha}_{\mathbf{k}n}|v_{\mathrm{SOC}}|\varphi^{\beta}_{\mathbf{k}n'}\rangle = \sum_{a}\sum_{lm}\sum_{l'm'}\delta_{ll'}\int_0^{R^a_{\mathrm{MT}}}drr^2 \times\frac{1}{(2M_{al}c)^2}\frac{1}{r}\frac{dv_a(r)}{dr}\langle lm\alpha|\mathbf{L}\cdot\boldsymbol{\sigma}|lm'\beta\rangle \times\left[A_{alm,n}(\mathbf{k})u^{\mathrm{L}}_{al}(r)+B_{alm,n}(\mathbf{k})\dot{u}^{\mathrm{L}}_{al}(r)\right]^* \times\left[A_{alm',n'}(\mathbf{k})u^{\mathrm{L}}_{al}(r)+B_{alm',n'}(\mathbf{k})\dot{u}^{\mathrm{L}}_{al}(r)\right], \tag{15}$$

where R^a_{MT} and $v_a(r)$ are the muffin-tin radius and the spherical part of the Kohn-Sham effective potential at atom a, respectively, and c is the speed of light. The spin-orbit coupling is sizable only close to the atomic nuclei, where the electron velocity is relativistic. It is negligible in the interstitial region, and we may replace the potential by its spherical part $v_a(r)$ in the muffin-tin spheres. Since the Hg chalcogenides, examined in this work, are nonmagnetic, we have omitted the spin index for the wave-function coefficients, the potential, and the radial functions. The relativistic mass M_{al} is given by

$$M_{al} = m_{\mathrm{e}} + \frac{1}{2c^2}[\epsilon_{al}-v_a(r)], \tag{16}$$

where m_{e} (= 1 in atomic units) is the electron rest mass and ϵ_{al} is the energy parameter used in the construction of the $u_{al}(r)$ and $\dot{u}_{al}(r)$. The extension to local orbitals is straightforward. In each iteration a new electron density is constructed from the wave functions in Eq. (11), which serves as input density for the next iteration. The procedure is iterated until convergence of the density is achieved.

We use the experimental zinc-blende lattice constants taken from Ref. 25 (HgS: 11.057 a.u.; HgSe: 11.497 a.u.; HgTe: 12.210 a.u.). We employ a plane-wave cutoff $|\mathbf{k}+\mathbf{G}|\leqslant G_{\max} = 5.0$ bohr^{-1} in the interstitial region and an angular-momentum cutoff $l\leqslant l_{\max} = 10$ in the spheres. Semicore d states of Se and Te as well as Hg $5p$ states are treated as valence orbitals by using suitably defined local orbitals. To describe high-lying states accurately, we also include for each atom two additional local orbitals per angular momentum up to $l = 4$.

The resulting spinor wave functions and energies are then used for the subsequent GW calculations. All occupied states, including the core states, are included in the exchange part of the self-energy, and semicore states are taken into account in both the polarization function and the correlation part of the self-energy. We employ an $8 \times 8 \times 8$ **k**-point sampling and include around 1000 unoccupied bands to compute the Green function and the polarization function.

III. RESULTS AND DISCUSSION

A. LDA band structure

Before presenting the results for the Hg-chalcogenide semiconductors, let us briefly review the understanding of the band structure of semiconductors with zinc-blende lattice. The s and p valence electrons of the two atoms in the unit cell form bonding and antibonding combinations, which generate the highest valence and the bottom conduction bands of the crystal, respectively. The top of the valence band is at the Γ point and arises from three p bonding orbitals, which are degenerate. Considering the spin of the electrons the top of the valence band is sixfold degenerate. The cubic crystal field imposed by the zinc-blende lattice splits the p band in the vicinity of the Γ point into a fourfold degenerate heavy- and a twofold degenerate light-hole band along high-symmetry lines Λ and Δ.

Spin-orbit interaction, and for the HgX compounds this means essentially the spin-orbit interaction of the chalcogenide anions S, Se, and Te, changes the band topology. It splits the top-most valence bands into two groups, the $p_{3/2}$ bands with a fourfold degeneracy at the center of the Brillouin zone and labeled Γ_8, using the appropriate double-group representations for the zinc-blende space group, and the $p_{1/2}$ bands, also called spin-orbit split-off bands, with degeneracy 2 and labeled Γ_7 states at the Γ point. The latter band connects to the neighboring high-symmetry points as the light-hole band would at the absence of spin-orbit interaction. Around the Γ point, the cubic crystal field splits the $p_{3/2}$ states into two twofold degenerate bands of $m_j = \pm 3/2$ and $m_j = \pm 1/2$ eigenstates. One takes the role of the heavy-hole ($m = \pm 3/2$) band across the high-symmetry lines and one the light-hole states around Γ.

Since the zinc-blende lattice lacks a center of inversion, the Dresselhaus effect[1] is expected to lift the degeneracies of bands along particular high-symmetry lines, with the consequence that the energy maximum of the valence band is slightly shifted off the center of the zone. However, the removal of the double degeneracy close to the center of the Brillouin zone by the effect of the linear terms in **k** is very small and is not considered here any further. For conventional II-VI compounds the conduction electrons are predominantly of antibonding s character and the state at the zone center is denoted by Γ_6.

The high nuclear number of Hg changes now the picture in two respects. The s electron has a high probability of presence in the vicinity of the nucleus, where the s electron experiences the deep Coulomb potential of Hg. The high speed of the electron associated with the deep potential leads to a considerable relativistic mass enhancement, which pulls the energy level of the s state down, changes the bonding-antibonding hybridization between s and p electrons, alters the band dispersions, and leads to the inverted band structure of the Hg compounds, where the Γ_6 state lies now below the Γ_8 state and as we will see below, in the case of LDA calculations applied to mercury compounds, it is also always below the Γ_7 state. In particular around the Γ point, $\mathbf{k} \cdot \mathbf{p}$ perturbation theory[37] tells us that the effective mass of the Γ_6, the Γ_7, and the light-hole Γ_8 state depends on matrix elements between s and p electrons and an energy denominator, in which the energy difference between the valence and conduction state enters. If the s state moves below one of the p ones, curvatures of the bands in the vicinity of the Γ_6, Γ_7, and the light-hole state can change sign and depending on the energy difference, effective electron masses change their absolute values.

The inversion of the band structure is facilitated by the contraction of the Hg s wave function that increases the screening of the Coulomb attraction of the nucleus and the mercury d states become shallower in energy. According to the zinc-blende space group, Hg d and chalcogenide p states can hybridize and the p electrons get slightly pushed up in energy, and a slight p-d antibonding character is mixed into the valence p states. This state repulsion decreases from HgS to HgTe and together with the decrease of the s-s and p-p bonding-antibonding splitting and the increased spin-orbit splitting of the valence p bands, when comparing the chemical trend from HgS to HgTe, explains then the subtle difference of the band topology around the Γ point of the mercury chalcogenides.

Now we turn to the calculated band structures shown in Figs. 1(a)–1(c) and in Figs. 2(a)–2(c) magnified around the Γ point focusing first on the LDA results. The band structures of the three compounds are very similar. HgSe and HgTe are semimetals, and β-HgS is a semiconductor with a small energy gap of 0.1 eV. In all cases, the Γ_6 state is the lowest valence state at the Γ point. Along the high-symmetry line between the Γ and the L point, the energy difference between the $m_j = \pm 3/2$ heavy-hole and $m_j = \pm 1/2$ light-hole band increases from HgS to HgTe due to the increase of the spin-orbit splitting. A closer look reveals also a small splitting of the heavy-hole band along that direction, which increases also when comparing HgS to HgSe and HgTe. This is due to the hybridization of the spin-orbit split p band with the spin-orbit split (2 eV) Hg d bands located at around -7.7 eV below the Fermi energy (outside the displayed energy range).

To analyze the band inversion, which results from a hybridization of s and p states as already mentioned, the contribution from the Hg 6s muffin-tin orbital is indicated by the size of the vertical bars along the LDA band dispersion. It can be seen that the orbital character is rather **k** dependent. At the Γ point, the lowest band in the figures (Γ_6) exhibits a large admixture of Hg 6s, which clearly shows the inverted band structure of these systems, while the fourfold degenerate Γ_8 and twofold degenerate split-off Γ_7 states, which lie above the Γ_6 state, are mainly composed of chalcogen p orbitals. Apart from a small region of **k** space around the Γ point, the lowest unoccupied band mainly consists of Hg 6s. The values of the inverse band gap and spin-orbit splitting are tabulated in Tables I and II. Results from previous studies and experiment are also shown for comparison.

B. GW band structure

Concerning the quasiparticle band structure, the self-energy correction results in three noticeable effects. First, there is a

TABLE I. Calculated inverse direct band gaps at selected high-symmetry **k** points in eV. At the Γ point the inverse band gap is defined as $E_g = E_{\Gamma_6} - E_{\Gamma_8}$. In parentheses we report the results obtained with the screened Coulomb interaction W calculated without spin-orbit coupling (see text).

	HgS		HgSe		HgTe	
	LDA	*GW*	LDA	*GW*	LDA	*GW*
Γ						
This work	−0.66	−0.02	−1.27	−0.58	−1.20	−0.60
		(−0.01)		(−0.57)		(−0.58)
Ref. 24			−1.27	−0.51		
Ref. 25	−0.62	+0.06	−1.23	−0.60	−1.17	−0.57
Ref. 38[a]	−0.573		−1.18		−1.025	
	−0.58		−1.26		−1.15	
Expt.	−0.15[b],−0.11[c]		−0.274[d]		−0.29 ± 0.02[e]	
					−0.30[f]	
L						
This work	+2.37	+3.28	+1.81	+2.67	+1.28	+1.95
		(+3.29)		(+2.69)		(+1.97)
Ref. 24				+2.9		
Expt.			+2.949,+2.971[g]		2.25[f]	
X						
This work	+5.40	+6.25	+5.00	+5.79	+4.03	+4.62
		(+6.26)		(+5.80)		(+4.65)
Expt.			+5.7[h]		+5.0[h]	

[a]Results with VASP (Ref. 39) and ABINIT (Ref. 40) at theoretical volumes.
[b]Reference 41.
[c]Reference 42.
[d]Reference 43.
[e]Reference 44.
[f]Reference 46.
[g]Reference 47.
[h]Reference 48.

significant upward shift of the Γ_6 state, which causes a flip in the sequence between the Γ_6 and Γ_7 state for HgTe as compared to the LDA result and which reduces in general the negative inverse band gaps at Γ, defined as $E_{\Gamma_6} - E_{\Gamma_8}$, by about 0.7 eV for all materials, giving a much better agreement with experiment. These results are in accordance with previous studies by Rohlfing and Louie[24] as well as Fleszar and Hanke.[25] Second, the lowest conduction band, which is primarily of Hg 6*s* character, is shifted up markedly except at the Γ point. This results in a strongly reduced effective mass as discussed later. Third, the energy gap of β-HgS formed by Γ_8 and Γ_7 valence and conduction states, respectively, increases to 0.2 eV.

As pointed out by Cardona *et al.*,[38] the fact that the LDA yields too deep conductionlike Γ_6 states in the Hg chalcogenides is related to the band-gap problem of the LDA. In a LDA band structure of a conventional zinc-blende semiconductor, the conduction band is located too close to the valence band so that states around the Γ point strongly hybridize with each other. A similar hybridization effect can be seen in Fig. 1, where the Γ_6 state at the top of the valence band acquires Hg 6*s* character, whereas the lowest conduction state Γ_7 is mainly of chalcogenide *p* character, giving rise to the inverted band structure. The LDA places the conductionlike Γ_6 state too low in energy, just as it would in the case of a normal zinc-blende semiconductor, where this state forms the conduction-band minimum. As the *GW* approximation for the self-energy is known to correct for the underestimation of the normal semiconductor band gap, one might expect that it also corrects for the too low placement of the Γ_6 states in LDA. Indeed, as Fig. 1 shows, states of Hg 6*s* character are shifted up markedly, reducing the absolute value of the inverse band gap considerably. One may say that the LDA overestimates the stability of the inverted band structure.

Comparing our results with experiment, it seems that the GWA still underestimates the inverse band gap for HgSe and HgTe by about 0.3 eV. Considering the large discrepancy (around 1 eV) between the LDA results and experiment, the remaining discrepancy between the *GW* results and experiment may be overcome by using a better reference one-particle system than LDA as starting point or by iterating the *GW* calculation. On the other hand, the discrepancy may be due to the shortcoming of the GWA itself. Indeed, by including a vertex correction derived from time-dependent LDA, Fleszar and Hanke obtained a 0.1–0.2-eV upward correction of the *GW* inverse band gaps.[25]

C. Effective mass

Figure 1 shows that the electron effective mass at the Γ point is considerably reduced by the self-energy correction. We have estimated the effective masses from our data points

TABLE II. Spin-orbit splitting at selected high-symmetry **k** points in eV. At the Γ point the splitting is defined as $\Delta = E_{\Gamma_8} - E_{\Gamma_7}$. The negative values in HgS mean that the Γ_7 split-off state is above the Γ_8 state. In parentheses we report the results obtained with the screened Coulomb interaction W calculated without spin-orbit coupling (see text).

	HgS		HgSe		HgTe	
	LDA	GW	LDA	GW	LDA	GW
Γ						
This work	−0.12	−0.19 (−0.19)	+0.23	+0.32 (+0.32)	+0.78	+0.91 (+0.91)
Ref. 24				+0.30		
Ref. 25	−0.12	−0.12	+0.23	+0.23	+0.80	+0.80
Ref. 38[a]	−0.111		+0.23		+0.783	
	−0.18		+0.34		+0.81	
Expt.			+0.39,+0.38[b]		+0.91±0.02[c]	
					+0.910[d]	
L						
This work	+0.04	+0.01 (+0.01)	+0.19	+0.24 (+0.24)	+0.54	+0.61 (+0.61)
Expt.			+0.27[e], +0.3[f]		+0.62[g], +0.75[f]	
X						
This work	+0.12	+0.14 (+0.14)	+0.01	< +0.01 (< +0.01)	+0.21	+0.22 (+0.22)
Expt.			+0.3[f]		+0.1-0.2[f]	

[a]Results with VASP (Ref. 39) and ABINIT (Ref. 40) at theoretical volumes.
[b]Reference 49.
[c]Reference 44.
[d]Reference 45.
[e]Reference 47.
[f]Reference 48.
[g]Reference 46.

and list them in Table III. The reduction of the effective mass in the case of HgSe was also found by Rohlfing and Louie.[24] The ratio between the quasiparticle effective mass m^{QP} and the LDA effective mass m^{LDA} for a given state is given by[50]

$$\frac{m^{\mathrm{QP}}_{\mathbf{k}\mu}}{m^{\mathrm{LDA}}_{\mathbf{k}\mu}} = \frac{1}{Z_{\mathbf{k}\mu}} \lim_{\mathbf{k}\to 0} \left[1 + \sum_i \frac{m^{\mathrm{LDA}}_{\mathbf{k}\mu}}{k_i} \frac{\partial \mathrm{Re}\Sigma(\mathbf{k}, E_{\mathbf{k}\mu})}{\partial k_i} \right]^{-1}, \quad (17)$$

where

$$Z_{\mathbf{k}\mu} = \left[1 - \frac{\partial \mathrm{Re}\Sigma(\mathbf{k},\omega)}{\partial \omega}\bigg|_{\omega = E_{\mathbf{k}\mu}} \right]^{-1} \quad (18)$$

is the quasiparticle renormalization factor. The experimental values of these materials are strongly dependent on electron concentration but typically $m \approx 0.03$.[42,49] The GWA clearly improves the agreement with experiment. The quasiparticle renormalization factor $Z_{\mathbf{k}\mu}$ is typically 0.7–0.8 giving $1/Z_{\mathbf{k}\mu} \approx 1.5$, and since $m^{\mathrm{QP}}_{\mathbf{k}\mu}/m^{\mathrm{LDA}}_{\mathbf{k}\mu} \approx 0.5$, we can conclude from the above equation that the **k** dependence of the self-energy must be strong, which is a result of the **k**-dependent orbital character of the lowest conduction band, changing from chalcogenide p to Hg 6s as we approach the Γ point.

D. Spin-orbit splitting

The spin-orbit splitting Δ at the Γ point is defined as $\Delta = E_{\Gamma_8} - E_{\Gamma_7}$. As displayed in Table II, the spin-orbit splittings of HgSe and HgTe are enhanced by about 0.1 eV as a result of the GW self-energy correction, bringing them closer to experiment. Since the spin-orbit splitting itself is of the same order of magnitude, this is a significant improvement, which has not been observed by Fleszar and Hanke,[25] who included the spin-orbit coupling perturbatively after the GW correction. Obviously, many-body renormalization effects not only affect the negative inverse band gap but also the spin-orbit splitting, even though the spin-orbit coupling is predominantly a one-particle phenomenon. Thus at least for compounds containing chemical elements with high nuclear numbers such as, for example, Hg, Tl, Pb, or Bi, a purely perturbative treatment of spin-orbit coupling is not sufficient, and the self-energy must be taken as a full 2 × 2 matrix in spin space as is done in this work.

E. Self-energy analysis

In order to analyze the self-energy effect on the inverse band gap and the spin-orbit splitting, we plot in Figs. 3(a) and 3(b),

TABLE III. Theoretical electron effective masses at the Γ point for [111] (Γ → L) and [100] (Γ → X) directions.

	HgS		HgSe		HgTe	
	LDA	GW	LDA	GW	LDA	GW
$m_{[111]}$	0.27	0.15	0.34	0.16	0.30	0.17
$m_{[100]}$	0.21	0.15	0.23	0.15	0.19	0.14

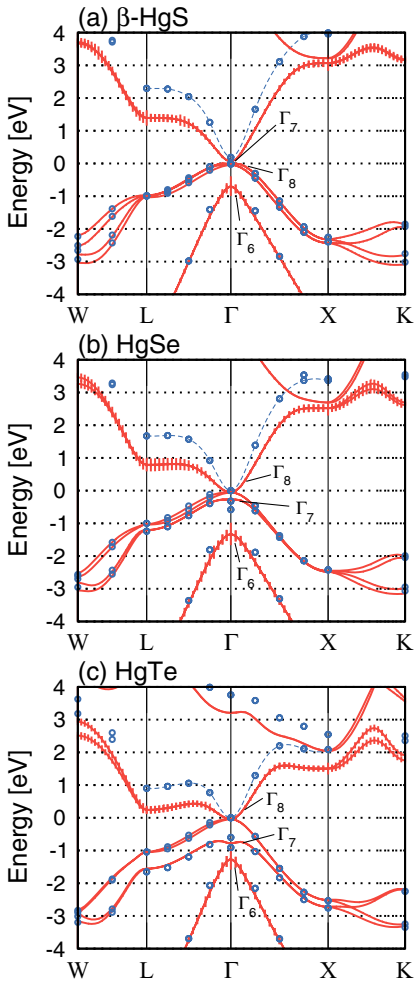

FIG. 1. (Color online) Band structures of HgX (X = S, Se, and Te) calculated with LDA (solid lines) and GW (circles). All calculations include spin-orbit coupling nonperturbatively. The vertical bars scale with the projection of the wave functions onto the Hg 6s state. The dashed lines are a guide to the eye.

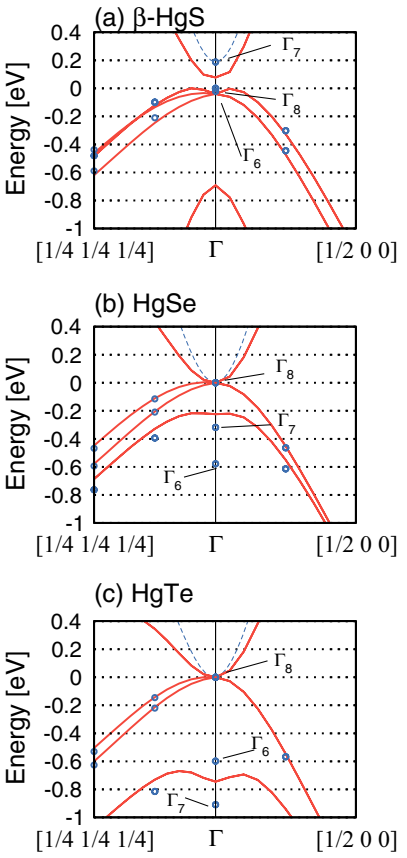

FIG. 2. (Color online) Band structure of HgX (X = S, Se, and Te) as shown in Fig. 1 magnified around the Γ point. Labels indicate GW results.

respectively, the exchange and correlation contributions to the self-energy correction for the Γ_6, Γ_7, and Γ_8 states. The exchange self-energy correction, which is defined as $\sum_{\alpha\beta}\langle\phi^{\alpha}_{\mathbf{k}\mu}|\Sigma^{\mathrm{x}}_{\alpha\beta} - v^{\mathrm{xc}}\delta_{\alpha\beta}|\phi^{\beta}_{\mathbf{k}\mu}\rangle$, has a pronounced effect on the quasiparticle band structure. The Γ_6 state shifts upward by around 2 eV, whereas the other two shift downward by 1–2 eV. The large upward shift can be understood by noticing that the Γ_6 state is mainly of conduction-band-like Hg 6s character. Therefore it has little overlap with the valence states so that this state experiences a much weaker exchange interaction than the other two states. This peculiar, strong **k** and band dependence of the self-energy correction is a very unusual but characteristic feature of the band inversion in these materials. It should be observed in other systems with inverted band structures, too. The exchange part of the self-energy correction has a profound effect on the spin-orbit splitting, which is reduced by about 1 eV in the case of HgS, while it is increased by as much as 1 eV for HgSe and HgTe. The inclusion of the correlation self-energy strongly compensates the large effect of the bare exchange, as shown in Fig. 3(b), but a small correction remains and yields values in good agreement with experiment, as we have seen in Table II. Obviously, the self-energy correction of the spin-orbit splitting is subject to a balance between the state-dependent exchange and correlation contributions, in much the same way as in the case of the band gap. As shown in Table II, the enhancement of the spin-orbit splitting can also be seen at the L and X points, and the calculated values agree well with experiments, except for the splitting at the X point of HgSe. The renormalization of the spin-orbit splitting due to the self-energy correction is also found with a two-dimensional Rashba model Hamiltonian by Chen and Raikh.[51]

To analyze the effect of spin-orbit coupling on the self-energy in more detail, we show in Tables I and II in parentheses results obtained with the screened Coulomb interaction W calculated without spin-orbit coupling. In these calculations, P and W are generated from LDA wave functions and energies obtained from a *one-shot* diagonalization of the spin-orbit-free Hamiltonian with the same effective potential as for the other calculations. For all other quantities, in particular the Kohn-Sham Green function in Eq. (5), we use the fully relativistic spinor wave functions. As can be seen, the difference to the original values is very small, on the order of ten meV. This indicates that virtual transitions into high-lying states yield the dominant contribution to screening so that spin-orbit effects, which are confined to a very small energy region around the

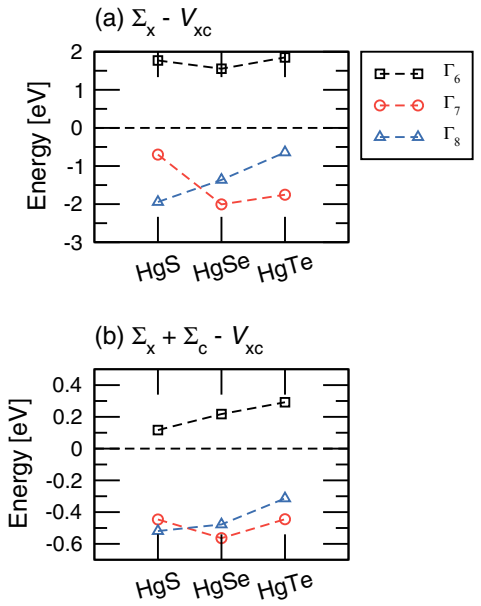

FIG. 3. (Color online) Self-energy correction for the states Γ_6, Γ_7, and Γ_8: (a) only bare exchange and (b) full GW correction. The lines are a guide to the eye.

Fermi energy, give only a minor correction. This also implies that the corrections of the negative inverse band gap and the spin-orbit splitting have their origin in the "static" part of the self-energy, i.e., the Green function in Eq. (5), which suggests that one may be able to simplify the GW calculations by including the effect of the spin-orbit coupling only in G, thus avoiding the time-consuming calculation of the polarization function with twice as many band states.

F. Ordering of states

Finally, we briefly mention the ordering of the states at the Γ point, which is still under debate, as obtained from the quasiparticle correction. We obtain from top to bottom $\Gamma_7 - \Gamma_8 - \Gamma_6$ in HgS, $\Gamma_8 - \Gamma_7 - \Gamma_6$ in HgSe, and $\Gamma_8 - \Gamma_6 - \Gamma_7$ in HgTe. In experiment, the ordering is $\Gamma_8 - \Gamma_6 - \Gamma_7$ in HgSe and HgTe. The discrepancy between theory and experiment in HgSe is most likely to be attributed to the still underestimated inverse gap in GW. The HgS case is more difficult to assess. Experimentally, the gap of HgS is negative,[41,42] indicating that HgS has an inverted band structure. In contrast, Fleszar and Hanke[25] showed that in HgS the Γ_6 state is above the Γ_8 state within the GWA, which indicates that HgS has a "normal" band structure, except for the negative spin-orbit splitting, with the ordering $\Gamma_7 - \Gamma_6 - \Gamma_8$. Moon and Wei[52] also obtained a normal band structure for HgS using the LDA and a semiempirical local potential. Their ordering is $\Gamma_6 - \Gamma_7 - \Gamma_8$, with a band gap of 0.30 eV. On the other hand, in our calculation Γ_6 is, in fact, slightly below the Γ_8 state, giving rise to an inverted band structure, in qualitative agreement with experiment. However, the inverse gap of -0.02 eV deviates somewhat from the experimentally found values of -0.15 eV, Ref. 41, and -0.11 eV, Ref. 42. Further experimental studies, including the determination of the sign of the spin-orbit splitting, would be helpful to settle this issue.

IV. CONCLUSIONS

In this paper, we have implemented a fully spin-dependent formulation of the GW approximation, which allows us to describe many-body renormalization effects that arise from spin-orbit coupling. This approach goes beyond a mere perturbative treatment within LDA and takes into account the spin off-diagonal elements of the Green function and the self-energy, which emerge as a result of the coupling of spatial and spin degrees of freedom. The core, valence, and conduction states of the reference one-particle system are treated fully relativistically as four-component spinor wave functions.

We have applied the scheme to quasiparticle calculations of mercury chalcogenides and found that the self-energy correction has a noticeable effect on their electronic band structures. These systems exhibit an inverted band structure due to strong relativistic effects. In LDA their band gaps are correctly predicted to be negative. However, quantitatively, they are far too negative compared to experiment, leading to an overestimated band inversion. In accordance with previous studies, we obtain a considerable quantitative improvement of the inverse band gap within the GW approximation, bringing the calculated values much closer to experiment.

Furthermore, we find an unprecedented many-body renormalization of the spin-orbit splitting that amounts to about 0.1 eV. This renormalization significantly improves the theoretical values with respect to experiment (with the exception of the spin-orbit splitting at the X point of HgSe). It is important to note that this renormalization effect is inaccessible in a pure perturbative treatment of spin-orbit coupling, and a full spin-dependent formulation is essential.

We have analyzed the self-energy correction of the inverse band gap and could trace it back to the inverted band structure: the lowest conduction band changes character from Hg 6*s* to chalcogenide *p* as one approaches the Γ point, whereas the valence band containing the Γ_6 state shows the opposite trend. This change of orbital character gives rise to a self-energy with a pronounced $\mathbf{k}$ dependence, which selectively pushes the conductionlike Γ_6 state up in energy, effectively reducing the inverse band gap and bringing it closer to experiment.

Another interesting finding is the reduction of the electron effective mass by a factor of 2 as compared with the LDA value. For the case of HgSe this was already reported in Ref. 24. We have shown that the origin of this reduction can also be attributed to the strong $\mathbf{k}$ dependence of the self-energy. We suggest further experimental studies on β-HgS semiconductors to settle finally the presence of an energy gap in this system.

We have investigated the effect of spin-orbit coupling on the screened interaction and found it to be minor in the systems studied, implying that the spin-orbit induced changes of the GW self-energy originate mainly from the single-particle Green function. This finding may allow for a simplification of GW calculations with spin-orbit coupling where the fully relativistic wave functions—including the spin-orbit coupling—are only used for the Green function, while the screened interaction is constructed from the scalar-relativistic, spin-orbit-free wave functions, thereby saving a large amount

of computational effort. It would be interesting to investigate if this finding also applies to other systems, e.g., the Ir-based systems such as Sr_2IrO_4, in which spin-orbit coupling modifies the band structure considerably.

The fully spin-dependent GWA presented here, in which spin-orbit coupling has been included in a consistent way, provides a reliable methodological approach to investigate the fine details of the electronic structure of topological insulators. These materials frequently contain chemical elements with high nuclear numbers, which are decisive for the physics induced by large spin-orbit interaction.

ACKNOWLEDGMENTS

Fruitful discussions with G. Bihlmayer are gratefully acknowledged. This work was supported by "Materials Design through Computics: Complex Correlation and Non-Equilibrium Dynamics,' A Grant in Aid for Scientific Research on Innovative Areas, and the Global Center-of-Excellence program (G-03) of MEXT Japan. We further acknowledge financial support from the Deutsche Forschungsgemeinschaft through the Priority Program 1145. Part of the calculations were performed at the Supercomputer Center of ISSP, Japan.

*reis@faculty.chiba-u.jp

[1]G. Dresselhaus, Phys. Rev. **100**, 580 (1955).
[2]Y. A. Bychkov and E. I. Rashba, JETP Lett. **39**, 78 (1984).
[3]Y. K. Kato, R. C. Myers, A. C. Gossard, and D. D. Awschalom, Science **306**, 1910 (2004).
[4]M. König, S. Wiedmann, C. Brüne, A. Roth, H. Buhmann, L. Molenkamp, X. Qi, and S. Zhang, Science **318**, 766 (2007).
[5]D. Hsieh, D. Qian, L. Wray, Y. Xia, Y. S. Hor, R. J. Cava, and M. Z. Hasan, Nature (London) **452**, 970 (2008).
[6]S. Chadov, X. Qi, J. Kübler, G. H. Fecher, C. Felser, and S. C. Zhang, Nat. Mater. **9**, 541 (2010).
[7]H. Lin, L. A. Wray, Y. Xia, S. Xu, S. Jia, R. J. Cava, A. Bansil, and M. Z. Hasan, Nat. Mater. **9**, 546 (2010).
[8]D. Xiao, Y. Yao, W. Feng, J. Wen, W. Zhu, X.-Q. Chen, G. M. Stocks, and Z. Zhang, Phys. Rev. Lett. **105**, 096404 (2010).
[9]W. Feng, D. Xiao, Y. Zhang, and Y. Yao, Phys. Rev. B **82**, 235121 (2010).
[10]W. Feng, D. Xiao, J. Ding, and Y. Yao, Phys. Rev. Lett. **106**, 016402 (2011).
[11]B. A. Bernevig, T. L. Hughes, and S.-C. Zhang, Science **314**, 1757 (2007).
[12]B. J. Kim, H. Jin, S. J. Moon, J.-Y. Kim, B.-G. Park, C. S. Leem, J. Yu, T. W. Noh, C. Kim, S.-J. Oh, J.-H. Park, V. Durairaj, G. Cao, and E. Rotenberg, Phys. Rev. Lett. **101**, 076402 (2008).
[13]A. Shitade, H. Katsura, J. Kuneš, X.-L. Qi, S.-C. Zhang, and N. Nagaosa, Phys. Rev. Lett. **102**, 256403 (2009).
[14]D. Pesin and L. Balents, Nat. Phys. **6**, 376 (2010).
[15]L. Hedin, Phys. Rev. **139**, A796 (1965).
[16]F. Aryasetiawan and O. Gunnarsson, Rep. Prog. Phys. **61**, 237 (1998).
[17]W. G. Aulbur, L. Joensson, and J. W. Wilkins, Solid State Phys. **54**, 1 (2000).
[18]F. Aryasetiawan and S. Biermann, Phys. Rev. Lett. **100**, 116402 (2008).
[19]F. Aryasetiawan and S. Biermann, J. Phys.: Condens. Matter **21**, 064232 (2009).
[20]I. A. Nechaev and E. V. Chulkov, Phys. Solid State **51**, 1772 (2009).
[21]V. P. Zhukov and E. V. Chulkov, Phys. Solid State **51**, 2211 (2009).
[22]S. Murakami, N. Nagaosa, and S.-C. Zhang, Phys. Rev. Lett. **93**, 156804 (2004).
[23]Liang Fu and C. L. Kane, Phys. Rev. B **76**, 045302 (2007).
[24]M. Rohlfing and S. G. Louie, Phys. Rev. B **57**, R9392 (1998).
[25]A. Fleszar and W. Hanke, Phys. Rev. B **71**, 045207 (2005).
[26]C. Friedrich, S. Blügel, and A. Schindlmayr, Phys. Rev. B **81**, 125102 (2010).
[27]C. Friedrich, A. Schindlmayr, and S. Blügel, Comput. Phys. Commun. **180**, 347 (2009).
[28][http://www.flapw.de/].
[29]J. P. Perdew and A. Zunger, Phys. Rev. B **23**, 5048 (1981).
[30]D. D. Koelling and B. N. Harmon, J. Phys. C **10**, 3107 (1977).
[31]A. H. MacDonald, W. E. Pickett, and D. D. Koelling, J. Phys. C **13**, 2675 (1980).
[32]C. Li, A. J. Freeman, H. J. F. Jansen, and C. L. Fu, Phys. Rev. B **42**, 5433 (1990).
[33]D. Singh, Phys. Rev. B **43**, 6388 (1991).
[34]E. E. Krasovskii, Phys. Rev. B **56**, 12866 (1997).
[35]C. Friedrich, A. Schindlmayr, S. Blügel, and T. Kotani, Phys. Rev. B **74**, 045104 (2006).
[36]C. Friedrich, M. C. Müller, and S. Blügel, Phys. Rev. B **83**, 081101 (2011).
[37]Evan O. Kane, J. Phys. Chem. Solids **1**, 249 (1957).
[38]M. Cardona, R. K. Kremer, R. Lauck, G. Siegle, A. Muñoz, and A. H. Romero, Phys. Rev. B **80**, 195204 (2009).
[39]G. Kresse and J. Hafner, Phys. Rev. B **47**, 558 (1993); **49**, 14251 (1994); G. Kresse and J. Furthmüller, Comput. Mater. Sci. **6**, 15 (1996); Phys. Rev. B **54**, 11169 (1996); [http://cms.mpi.univie.ac.at/vasp/].
[40]X. Gonze, B. Amadon, P.-M. Anglade, J.-M. Beuken, F. Bottin, P. Boulanger, F. Bruneval, D. Caliste, R. Caracas, M. Cote, T. Deutsch, L. Genovese, Ph. Ghosez, M. Giantomassi, S. Goedecker, D. R. Hamann, P. Hermet, F. Jollet, G. Jomard, S. Leroux, M. Mancini, S. Mazevet, M. J. T. Oliveira, G. Onida, Y. Pouillon, T. Rangel, G.-M. Rignanese, D. Sangalli, R. Shaltaf, M. Torrent, M. J. Verstraete, G. Zerah, and J. W. Zwanziger, Comput. Phys. Commun. **180**, 2582 (2009); X. Gonze, G.-M. Rignanese, M. Verstraete, J.-M. Beuken, Y. Pouillon, R. Caracas, F. Jollet, M. Torrent, G. Zerah, M. Mikami, Ph. Ghosez, M. Veithen, J.-Y. Raty, V. Olevano, F. Bruneval, L. Reining, R. Godby, G. Onida, D. R. Hamann, and D. C. Allan, Z. Kristallogr. **220**, 558 (2005); [http://www.abinit.org/].
[41]R. Zallen and M. Slade, Solid State Commun. **8**, 1291 (1970).
[42]K. Dybko, W. Szuszkiewicz, E. Dynowska, W. Paszkowicz, and B. Witkowska, Physica B **256–258**, 629 (1998).
[43]M. von Truchseß, A. Pfeuffer-Jeschke, C. R. Becker, G. Landwehr, and E. Batke, Phys. Rev. B **61**, 1666 (2000).
[44]N. Orlowski, J. Augustin, Z. Golacki, C. Janowitz, and R. Manzke, Phys. Rev. B **61**, R5058 (2000).

[45]C. Janowitz, N. Orlowski, R. Manzke, and Z. Golacki, J. Alloys Compd. **328**, 84 (2001).
[46]D. J. Chadi, J. P. Walter, M. L. Cohen, Y. Petroff, and M. Balkanski, Phys. Rev. B **5**, 3058 (1972).
[47]S. Einfeldt, F. Goschenhofer, C. R. Becker, and G. Landwehr, Phys. Rev. B **51**, 4915 (1995).
[48]W. J. Scouler and G. B. Wright, Phys. Rev. **133**, A736 (1964).
[49]*Numerical Data and Functional Relationships in Science and Technology*, Landolt-Börnstein, Group III, Vol. 41, Part b, edited by O. Madelung, U. Rössler, and M. Schulz (Springer, Berlin, 1999).
[50]M. Oshikiri, F. Aryasetiawan, Y. Imanaka, and G. Kido, Phys. Rev. B **66**, 125204 (2002).
[51]G.-H. Chen and M. E. Raikh, Phys. Rev. B **60**, 4826 (1999).
[52]C.-Y. Moon and S.-H. Wei, Phys. Rev. B **74**, 045205 (2006).